Published in final edited form as:
Nat Genet. 2019 December 23; 51(6): 990–998. doi:10.1038/s41588-019-0413-z.

MTHFD1 interaction with BRD4 links folate metabolism to transcriptional regulation

Sara Sdelci[1,#], **André F. Rendeiro**[1], **Philipp Rathert**[2,$], **Wanhui You**[1,3], **Jung-Ming G. Lin**[1], **Anna Ringler**[1,3], **Gerald Hofstätter**[1,3], **Herwig P. Moll**[4], **Bettina Gürtl**[1], **Matthias Farlik**[1], **Sandra Schick**[1,3], **Freya Klepsch**[1], **Matthew Oldach**[1], **Pisanu Buphamalai**[1], **Fiorella Schischlik**[1], **Peter Májek**[1], **Katja Parapatics**[1], **Christian Schmidl**[1,^], **Michael Schuster**[1], **Thomas Penz**[1], **Dennis L. Buckley**[5], **Otto Hudecz**[6], **Richard Imre**[6], **Shuang-Yan Wang**[7,8], **Hans Michael Maric**[7,8], **Robert Kralovics**[1,9], **Keiryn L. Bennett**[1], **Andre C. Müller**[1], **Karl Mechtler**[2], **Jörg Menche**[1], **James E. Bradner**[5], **Georg E. Winter**[1], **Kristaps Klavins**[1], **Emilio Casanova**[4,10], **Christoph Bock**[1,9,11], **Johannes Zuber**[2,12], **Stefan Kubicek**[1,4,*]

[1]CeMM Research Center for Molecular Medicine of the Austrian Academy of Sciences. Lazarettgasse 14, 1090 Vienna, Austria

[2]Research Institute of Molecular Pathology (IMP), Vienna Biocenter (VBC), 1030 Vienna, Austria

[3]Christian Doppler Laboratory for Chemical Epigenetics and Antiinfectives, CeMM Research Center for Molecular Medicine of the Austrian Academy of Sciences, Vienna, Austria

[4]Department of Physiology, Center of Physiology and Pharmacology & Comprehensive Cancer Center (CCC), Medical University of Vienna, Vienna, Austria

[5]Department of Medical Oncology, Dana-Farber Cancer Institute, Harvard Medical School, Boston, MA 02215

[*]Correspondence to: Stefan Kubicek, CeMM Research Center for Molecular Medicine of the Austrian Academy of Sciences, Lazarettgasse 14 AKH BT 25.3 1090 Vienna, Austria. Phone +43-1/40160-70 036, Fax +43-1/40160-970 000, skubicek@cemm.oeaw.ac.at.
[#]Current address: Centre for Genomic Regulation (CRG), The Barcelona Institute of Science and Technology, 08003 Barcelona, Spain.
[$]Current address: Biochemistry Department, University Stuttgart, 70569 Stuttgart, Germany.
[^]Current address: Regensburg Center for Interventional Immunology (RCI), University Regensburg and University Medical Center Regensburg, Germany.

Data Availability

Next-generation sequencing data have been deposited to NCBI GEO (accession GSE105786), proteomic data have been deposited to PRIDE (accessions PXD012715, PXD013090).

Author Contributions

S.S. and S.K. conceived the project and designed the study; S.S. and G.H. performed the gene-trap screen. F.S. and R.K. analyzed gene-trap screening data; P.R., O.H., R.I., K.M., and J.Z. performed and analyzed the BRD4 interactome screen; S.S., W.Y., G.L., G.H., A.Ri., and S.Sch. performed biochemical and cell biological experiments and generated ChIP and metabolomic samples; K.K, B.G. and A.M. performed and analyzed proteomic and metabolomic experiments. A.Re., M.O., C.S, M.F., M.S., T.P., and C.B. performed next-generation sequencing and analyzed ChIP data; F.K. performed molecular modeling; P.M., M.O., K.P., and K.L.B. generated and analyzed chromatin-bound proteomes; P.B. and J.M. analyzed metabolomic data; S.Y.W. and H.M.M. designed, performed and analyzed peptide microarray studies, D.L.B., J.E.B., and G.E.W. designed, synthesized and provided degronimids; H.P.M. and E.C. designed and conducted mouse xenograft studies. S.S. and S.K. wrote the manuscript with input from all co-authors.

Competing Interests

S.S. and S.K. have filed patent application WO/2018/087401 based on findings described in this manuscript. J.E.B is now a shareholder and executive of Novartis AG, and formerly the founder of the BET bromodomain focused company Tensha (acquired by Roche).

Europe PMC Funders Author Manuscripts

[6]Institute of Molecular Biotechnology of the Austrian Academy of Sciences (IMBA), Vienna Biocenter (VBC), 1030 Vienna, Austria

[7]Department of Biotechnology and Biophysics, Biocenter, University of Würzburg, 97074 Würzburg, Germany

[8]Institute of Structural Biology, Rudolf Virchow Center for Experimental Biomedicine, University of Würzburg, 97080 Würzburg, Germany

[9]Department of Laboratory Medicine, Medical University of Vienna, 1090 Vienna, Austria

[10]Ludwig Boltzmann Institute for Cancer Research (LBI-CR), Vienna, Austria

[11]Max Planck Institute for Informatics, 66123 Saarbrücken, Germany

[12]Medical University of Vienna, Vienna BioCenter (VBC), 1030 Vienna, Austria

Europe PMC Funders Author Manuscripts

Abstract

The histone acetyl-reader BRD4 is an important regulator of chromatin structure and transcription, yet factors modulating its activity have remained elusive. Here we describe two complementary screens for genetic and physical interactors of BRD4, which converge on the folate pathway enzyme MTHFD1. We show that a fraction of MTHFD1 resides in the nucleus, where it is recruited to distinct genomic loci by direct interaction with BRD4. Inhibition of either BRD4 or MTHFD1 results in similar changes in nuclear metabolite composition and gene expression, and pharmacologic inhibitors of the two pathways synergize to impair cancer cell viability *in vitro* and *in vivo*. Our finding that MTHFD1 and other metabolic enzymes are chromatin-associated suggests a direct role for nuclear metabolism in the control of gene expression.

Introduction

BRD4 is an important chromatin regulator with roles in gene regulation, DNA damage, cell proliferation and cancer progression[1–4]. The protein is recruited to distinct genomic loci by the interaction of its tandem bromodomains with acetylated lysines on histones and other nuclear proteins[5]. There, BRD4 acts as a transcriptional activator by P-TEFb-mediated stimulation of transcriptional elongation[6]. The activating function of BRD4 on key driver oncogenes like *MYC* have made this epigenetic enzyme an important therapeutic target in both *BRD4*-translocated and *BRD4* wild-type cancers[3,7–12], and at least seven bromodomain inhibitors have reached the clinical stage[13]. Genome-wide studies have identified the role of BRD4-induced epigenetic heterogeneity in cancer cell resistance[14], and factors defining BRD4 inhibitor response[15,16]. However, despite its clinical importance and the broad role of BRD4 in chromatin organization, surprisingly little is known about factors that are directly required for BRD4 function. To systematically expand the list of known BRD4 interactors[5] and to characterize proteins directly required for BRD4 function, we developed a strategy of two complementary screens for genetic and physical partners of BRD4. The two approaches converge on a single factor, methylenetetrahydrofolate dehydrogenase 1 (MTHFD1). Our description of a transcriptional role for this C-1-tetrahydrofolate synthase highlights a direct connection between nuclear folate metabolism and cancer regulation.

Results

A genetic loss-of-function screen for BRD4 pathway genes identifies MTHFD1

We recently generated reporter for epigenetic drug screening (REDS) cell lines that respond to inhibition of BRD4 with the expression of red fluorescent protein (RFP) (Supplementary Fig. 1)[17]. The near-haploid genotype of these cells, originating from the chronic myeloid leukemia cell line KBM7, makes them ideally suited for gene-trap genetic screens[18,19]. We therefore tested several REDS clones for their karyotype and confirmed the haploidity of one clone, REDS1. This clone, which harbors a single RFP integration in the first intron of *CDKAL1,* robustly induced RFP expression when treated with the BRD4 inhibitor (*S*)-JQ1 or with short hairpin RNAs (shRNAs) targeting *BRD4* mRNA (Supplementary Fig. 1). We then performed a gene-trap-mediated genetic screen on this clone in order to identify new functional interactors of BRD4 (Fig. 1a). The high specificity of the screening system relies on a rapid gain of RFP signal, which indicates chromatin changes phenocopying BRD4 inhibition. Therefore, the expression of RFP upon a specific gene knock-out suggests that the gene targeted is either directly required for BRD4 function or independently involved in chromatin remodeling at BRD4-dependent loci. We infected REDS1 cells with a gene-trap virus that results in the integration of a splice acceptor site followed by green fluorescent protein (GFP) reporter gene and a polyadenylation signal, thereby causing in the premature termination typically after the first exon and thus loss of function of target genes. We then expanded cells for two weeks, sorted double-positive cells (RFP^+/GFP^+) (Fig. 1b), extracted genomic DNA from this population, amplified gene-trap integration sites and sequenced and mapped them onto the genome. Two prominent protein-coding genes emerged from the analysis of these data for the number and orientation of integrations: *MTHFD1* and *MDC1* (mediator of DNA damage checkpoint 1) (Fig. 1c, Supplementary Fig. 2 and Supplementary Table 1). *MDC1*, a gene involved in DNA repair, can be linked to BRD4 biology indirectly through the insulator role of the short isoform of BRD4 during DNA damage signaling[2]. To validate *MTHFD1* as a genetic interactor of BRD4, REDS1 cells were treated with three different shRNAs resulting in 44-92% knock-down of MTHFD1 (Fig. 1d). All three hairpins induced RFP expression, and the effect size correlated with their knock-down efficiency (Fig. 1e-f). To rule out clone-specific effects, we repeated the same experiment in the diploid REDS3 clone and obtained comparable results (Supplementary Fig. 2).

MTHFD1 is recruited to chromatin by physical interaction with BRD4

In a second complementary profiling approach, we used proteomics to identify BRD4 interactors in K-562, MOLM-13, MV4-11 and MEG-01 leukemia cell lines (Fig. 2a and Supplementary Fig. 3). Only 13 proteins commonly interacted with BRD4 in all four cell lines. This set comprised several chromatin proteins like BRD3, LMNB1 and SMC3 and additionally included MTHFD1, the folate pathway enzyme identified in the genetic screen. The physical interaction between BRD4 and MTHFD1 was confirmed in the four leukemia cell lines (Fig. 2b) and all additional cell lines tested (Supplementary Fig. 3). The inverse experiment using MTHFD1 as bait confirmed the interaction with BRD4 and other proteins important for transcription (Supplementary Fig. 3). On tiling peptide microarrays MTHFD1 interacted with several BRD4-derived peptides, particularly those of the bromodomains (Supplementary Fig. 3). Similarly, several potential interaction sites were identified on

MTHFD1, and acetylation of MTHFD1-derived peptides on the known modification sites K56 and K819 increased the binding of BRD4. Recombinant MTHFD1 and a MTHFD1(K56ac) peptide inhibited the interaction between BRD4 and acetylated histone peptides (Supplementary Fig. 3). In cellular pull-down assays all BRD4 isoforms interacted with full-length MTHFD1 but not with the dehydrogenase/cyclohydrolase or formyltetrahydrofolate-synthase domains alone (Supplementary Fig. 4). The MTHFD1(K56A) mutation, which mimics the uncharged acetylated state, enhanced interaction with BRD4, while the mutation of the same residue to a charged arginine reduced the interaction. An N-terminal BRD4(1-480) fragment harboring both bromodomains was sufficient for the interaction with full-length MTHFD1, and the double bromodomain mutant GFP-BRD4 N140F/N433F showed drastically reduced binding to FLAG-MTHFD1 (Supplementary Fig. 4). In summary, these biochemical data are consistent with the interaction between the proteins occurring on several specific contact points, enhanced by binding of the BRD4 bromodomains to acetylated lysines on the surface of MTHFD1. Future studies are needed to structurally resolve the configuration of chromatin-bound MTHFD1 and to elucidate the impact of BRD4-dependent condensates[20,21] on the interaction.

While BRD4 is localized almost exclusively to the nucleus, folate metabolism is considered to occur in the cytoplasm and mitochondria[22]. Nuclear import of folate pathway enzymes including MTHFD1 has been described only recently[23,24]. Nuclear versus cytosolic fractionation of HAP1, KBM7 and HEK293T cells indicated that a fraction of MTHFD1 resides in the nucleus in all three cell lines (Fig. 2c). MTHFD1 pull-downs in the cytosolic and nuclear fractions of HAP1, KBM7 and HEK293T revealed that the interaction with BRD4 was restricted to the nucleus (Fig. 2c). With the nucleus confirmed as the interaction site of BRD4 and MTHFD1, we asked whether the BRD4-MTHFD1 complex was chromatin-bound or rather found in the soluble nuclear faction. We prepared chromatin extracts comprising tightly DNA-bound proteins from HAP1 cells and checked for the presence of BRD4 and MTHFD1 by western blot. Both proteins were clearly detectable in the chromatin-bound fraction (Fig. 2d). To probe whether BRD4 recruits MTHFD1 to chromatin, we treated HAP1 cells with the small molecule degronimids dBET1[25] and dBET6[4]. Two-hour treatment with these compounds resulted in the near-total ablation of BRD4 from chromatin. Under these conditions MTHFD1 was lost from chromatin, with remaining levels correlating with the amount of BRD4 (Fig. 2d), suggesting that BRD4 is the main factor recruiting MTHFD1 to chromatin. We further observed that methotrexate (MTX), an antifolate acting primarily on DHFR, caused a similar depletion of chromatin-associated MTHFD1, while it did not affect BRD4 levels. A possible explanation is direct competition between BRD4 and MTX for binding to the MTHFD1 substrate pocked containing K56ac. Importantly, BRD4 degradation or MTX treatment did not impair MTHFD1 nuclear localization (Fig. 2e), suggesting that while nuclear import of MTHFD1 is otherwise mediated, the interaction with BRD4 accounts for the recruitment of MTHFD1 to chromatin. To ensure cell-type independence, we confirmed that BRD4 degradation results in loss of MTHFD1 from chromatin in five additional cell lines (Fig. 2f-g).

Colocalization of MTHFD1 and BRD4 regulates gene expression

Having characterized BRD4-dependent chromatin recruitment of MTHFD1, we aimed to identify the genomic location of MTHFD1 binding by mapping the binding sites of the enzyme by ChIP-seq experiments in HAP1 cells. To control for antibody specificity, we generated MTHFD1-null HAP1 cells by CRISPR-Cas9 genome editing (Fig. 3a and Supplementary Fig. 5). MTHFD1 was detected at distinct genomic loci and signal was lost in MTHFD1 knock-out cells (Fig. 3b). In line with the proteomic experiments, the vast majority of MTHFD1 binding sites overlapped with BRD4 binding sites at promoter and enhancer regions, where H3K27ac was also enriched (Fig. 3c and Supplementary Fig. 6). Importantly, MTHFD1 chromatin binding was also lost after acute BRD4 degradation by 2 h treatment with dBET6 (Supplementary Fig. 7), suggesting a widespread role of MTHFD1 in chromatin regulation. Transcriptome analysis of HAP1 cells treated with BRD4 inhibitors, degraders and antifolates, as well as genetic perturbation by knock-down of BRD4 and knock-down/out of MTHFD1 validated the respective perturbation (Supplementary Fig. 8). While MTHFD1 knock-out resulted in expression changes of additional genes in the folate pathway, the more acute perturbations by compounds and shRNAs caused only minor changes in these genes. On the whole transcriptome level, we observed agreement in gene expression changes of compounds targeting BRD4 and antifolates, as well as between the genetic perturbation of BRD4 and MTHFD1 (Fig. 3d-e). Both MTHFD1 and BRD4 binding sites were enriched in promoters of genes with transcriptional functions (Supplementary Fig. 6), and combined analysis of chromatin binding and transcriptome changes revealed that genes bound by either protein were more highly expressed compared to similar genes without binding as detected by ChIP-seq (Supplementary Fig. 8). Both MTHFD1 and BRD4 were enriched at promoters of genes that were downregulated following knock-down of either of these proteins (Fig. 3f and Supplementary Fig. 8). The correlation between transcriptional effects of BET inhibitors and antifolates, as well as between knock-down of MTHFD1 and BRD4 was conserved in K-562 and A549 cells, suggesting cell type independence (Supplementary Fig. 9).

Loss of MTHFD1 or BRD4 result in similar metabolic changes

MTHFD1 is a C-1-tetrahydrofolate synthase that catalyzes three enzymatic reactions in folate metabolism, resulting in the interconversion of tetrahydrofolate, 10-formyltetrahydrofolate (10-CHO-THF), 5,10-methenyltetrahydrofolate (5,10-CH=THF) and 5,10-methylenetetrahydrofolate (5,10-CH2-THF) (Fig. 4a). These folates are key intermediates of one carbon metabolism and provide activated C1 groups for the biosynthesis of purines, pyrimidines and methionine. Biosynthesis of these three major classes of C1 metabolism products is considered to occur predominantly in the cytoplasm and mitochondria of mammalian cells[22], but we detected not only MTHFD1 but also several other enzymes required for nucleotide biosynthesis in the tightly chromatin-associated protein fraction in K-562 and HAP1 cells (Fig. 4a-b and Supplementary Table 2). To test whether BRD4 might affect MTHFD1 enzymatic activity, we used enzyme assays with recombinant protein in the presence of either full-length BRD4 or only the first bromodomain. We observed that full-length BRD4 boosted the activity of MTHFD1 to convert THF to 5,10-CH=THF (Fig. 4c).

We next asked whether inhibition of BRD4 or MTHFD1 altered nuclear metabolite composition. To as much as possible reduce technical challenges by fast diffusion rates and unselective metabolite loss through the nuclear pore, we used a protocol of rapid nuclei isolation after knock-down of either BRD4 or MTHFD1, and analyzed the nuclear metabolome relative to a non-targeting control hairpin. In total, we detected 2,851 metabolites, of which over 400 were significantly changed in one of the conditions. We observed strong correlation between the nuclear metabolomes in BRD4 and MTHFD1 knock-down conditions, particularly for metabolites in the purine, pyrimidine and methionine biosynthesis pathways (Fig. 4d, Supplementary Fig. 10). The direct MTHFD1 product 5,10-CH2-THF and most of the precursors for *de novo* nucleoside and nucleotide biosynthesis were depleted in both conditions, whereas the vast majority of free bases, nucleosides and nucleotides were increased. Furthermore, the trend for similar changes in nuclear metabolite composition was also noticeable in cells treated with small molecules dBET1 and MTX (Supplementary Fig. 10). BET inhibitors and MTX caused highly correlated characteristic changes specifically in the nuclear folate pool that were not observed with other cytotoxic compounds (Supplementary Fig. 10). Overall, a common nuclear metabolite signature for the inhibition of MTHFD1 and of BRD4 is evident, indicating a crosstalk between BRD4-dependent epigenetic regulation and folate metabolism. To test whether MTHFD1-derived metabolites are converted into nucleotides and incorporated into RNA, we treated cells with stable isotope labeled ^{13}C-formate, a cosubstrate for the conversion of THF to 10-CHO-THF. Within two hours we observed label incorporation into the direct MTHFD1 products 5,10-CH=THF and 5,10-methylenetetrahydrofolate 5,10-CH2-THF in wild-type HAP1 cells (Supplementary Fig. 10f). In MTHFD1 knock-out HAP1 cells, both the levels and the relative label incorporation of these metabolites were strongly reduced. We then isolated and hydrolyzed total cellular RNA after 24 h of ^{13}C-formate treatment. In wild-type HAP1 cells we observed significant label incorporation in purine but not pyrimidine nucleotides, which was absent in MTHFD1 knock-out cells (Fig. 4e). We therefore reconstituted MTHFD1 knock-out cells with either wild-type MTHFD1 or versions of the enzyme with constitutive nuclear localization (NLS) and nuclear export (NES) signals (Supplementary Fig. 11). Wild-type and NLS MTHFD1 resulted in label incorporation to levels comparable to HAP1 WT cells. In contrast, cytoplasm-enriched MTHFD1-NES lower levels of formate-derived purine bases incorporated into RNA, arguing for a nuclear-specific role of MTHFD1 (Fig. 4f).

Antifolates synergize with BRD4 inhibitors in diverse cancer models

Based on the similarities in nuclear metabolite composition following loss of MTHFD1 and BRD4, we speculated that antifolates might synergize with BRD4 inhibitors. To test this hypothesis, we treated REDS cells with (*S*)-JQ1 and MTX alone and in combination. Co-treatment with MTX remarkably amplified the basal RFP signal given by low doses of (*S*)-JQ1 alone (Fig. 5a). These results indicate that the chromatin remodeling process can be enhanced when inhibiting BRD4 and MTHFD1 together, emphasizing the role of folate metabolites in epigenetic regulation. We next tested whether this drug synergy also affected cancer cell survival. We selected six cell lines including four cell lines described as not sensitive to BRD4 inhibition, plus KBM7 and HAP1 cells (Supplementary Fig. 12). Dose response curves confirmed the low sensitivity of these cell lines to (*S*)-JQ1 treatment and a

moderate to low sensitivity to MTX treatment (Supplementary Fig. 12). In contrast to the poor response to (*S*)-JQ1 and MTX individual treatments, the combination of both drugs efficiently impaired cell viability in all six cell lines tested (Fig. 5b and Supplementary Fig. 12). Toxicity was observed at concentrations without any single-agent activity, indicating strong synergy between the two treatments, which was confirmed by calculating synergy indices according to the Bliss independence model[26] (Supplementary Fig. 12d). To exclude possible off-target effects of MTX, we treated the cell line showing the strongest drug synergism, A549, with shRNA for MTHFD1 and demonstrated increased sensitivity to (*S*)-JQ1 (Supplementary Fig. 12e). In addition, MTHFD1 knock-out HAP1 null cells responded with the induction of apoptosis at lower concentrations of (*S*)-JQ1 and MTX compared to WT cells (Supplementary Fig. 12). We further established that BET bromodomain inhibitors can be combined with antifolates *in vivo* to specifically inhibit cancer cell proliferation without exerting general toxicity. When we treated an A549 xenograft mouse model[27] with MTX and (*S*)-JQ1 alone and in combination, tumor growth was not impaired by either of the individual compounds, but arrested when the two inhibitors were given together (Fig. 5c-e).

Discussion

In contrast to nuclear ATP and acetyl-CoA biosynthesis[28,29], a direct role of folate pathway enzymes in the control of gene expression has not been comprehensively investigated. Here we characterize a transcriptional role for nuclear folate metabolism based on the genetic and biochemical interaction of MTHFD1 with BRD4. A fraction of MTHFD1 has previously been shown reside in the nucleus, where it is critical for thymidylate biosynthesis and protection from DNA damage response following folate deficiency[23,30–32]. Here we show that MTHFD1 binds chromatin in a BRD4-dependent manner at distinct genomic loci, where it controls gene expression and maintains a pool of folate metabolites in the nucleus. Interestingly, we identified not only MTHFD1 but also the other enzymes of *de novo* nucleotide biosynthesis pathway physically bound to chromatin. These enzymes were also detected in a recent large-scale chromatin proteomics study[33] and the purine pathway enzymes SHMT and ADE2 have been described as direct interactors of the BRD4 bromodomains[34]. Purine nucleotides are also the metabolites we find most dramatically changed following loss of either BRD4 or MTHFD1. While purine biosynthesis is generally considered to be localized exclusively to the cytoplasm, early work has shown that radioactive formate can be incorporated into RNA purine bases by isolated nuclei[35]. Future experiments will need to carefully evaluate the enzymatic activity of chromatin-bound nucleotide biosynthetic enzymes to uncover if certain steps of the pathway can also occur within the nucleus. In addition to the direct requirement of nucleotides for transcription, alterations in thymidylate and purine biosynthesis downstream of MTFHD1 might also cause nucleotide stress, which is known to impair P-TEFb activation and transcriptional elongation via upregulation of HEXIM1[36]. We hypothesize that BRD4-dependent MTHFD1 recruitment is needed to support local availability of one-carbon metabolites for full transcriptional activation of certain BRD4-target genes needed for cancer cell proliferation. Our finding thus adds to the growing list of metabolic enzymes and metabolites with roles in regulation of chromatin structure and transcription[37–40].

Due to its fundamental role in cell proliferation *via* nucleic acid biosynthesis, folate metabolism has been widely investigated in cancer biology. Several small molecules, including MTX, that target different enzymes of the folate pathway[41] have been developed. These antifolates are considered to act by inhibiting cell division, DNA/RNA synthesis and repair and protein synthesis[42]. Our findings suggest an additional 'targeted' mode of these classical chemotherapeutic drugs, which could enable better stratification and treatment regimens for cancer patients. Furthermore, we suggest combination of antifolates with BRD4 inhibitors as possible treatment for particularly aggressive cancers, potentially opening the avenue for more successful therapies.

Methods

Detailed information on experimental design and reagents can be found in the Life Sciences Reporting Summary.

Cell culture and transfection

KBM7 (human chronic myelogenous leukemia), MV4-11 (biphenotypic B myelomonocytic leukemia), MEG-01 (human chronic myelogenous leukemia), K-562 (human chronic myelogenous leukemia) and HAP1 (KBM7-derived) cell lines were cultured in Iscove's Modified Dulbecco's Medium (IMDM, Gibco), supplemented with 10% Fetal Bovine Serum (FBS; Gibco). HEK293T (human embryonic kidney) and HeLa (cervix adenocarcinoma) cell lines were cultured in Dulbecco's Modified Eagles Medium (DMEM, Gibco) supplemented with 10% FBS. MOLM-13 (human acute monocytic leukemia), NOMO-1 (human acute monocytic leukemia) and A549 (lung carcinoma) cell lines were cultured in RPMI-1640 (Roswell Park Memorial Institute, Gibco) supplemented with 10% FBS. All the mentioned cell lines were incubated in 5% CO_2 atmosphere at 37°C.

HEK293T cells were transfected with Lipofectamine 2000 (Invitrogen) according to the manufacturer's instructions.

The Retroviral Gene-Trap vector (pGT-GFP; see below) was a kind gift from Dr. Sebastian Nijman (Oxford, UK). GFP-MTHFD1 plasmid was a kind gift from Prof. Patrick Stover, Director of the Division of Nutritional Sciences, Cornell University (Ithaca, NY).

Western blot and immunoprecipitation

For Western blot, proteins were separated on polyacrylamide gels with SDS running buffer (50 mM Tris, 380 mM Glycine, 7 mM SDS) and transferred to nitrocellulose blotting membranes. All membranes were blocked with blocking buffer (5% (m/v) milk powder (BioRad) in TBST (Tris-buffered saline with Tween: 50 mM Tris (tris (hydroxymethyl)aminomethane), 150 mM NaCl, 0,05% (v/v) Tween 20, adjusted to pH 7.6). Proteins were probed with antibodies against BRD4 (ab128874, 1:1,000, Abcam), Actin (ab16039, 1:1,000, Abcam), MTHFD1 (ab70203, Abcam; H120, Santa Cruz; A8, Santa Cruz. All used at 1:1,000), MTHFD1L (ab229708, 1:1,000, Abcam), MTHFD2 (ab151447, 1:1,000, Abcam), GFP (G10362, 1:1,000, Life Technology), RCC1 (C-20, 1:1,000, Santa Cruz), β-Tubulin (T-4026, 1:1,000, Sigma), SHMT1 (ab186130, 1:1,000, Abcam), SHMT2 (ab180786, 1:1,000, Abcam), DHFR (ab49881, 1:1,000, abcam), Lamin-B (ab16048,

1:1,000, Abcam), VDAC-1 (ab15895, 1:1,000, Abcam) and H2B (ab156197, 1:1,000, Abcam) and detected by HRP (horseradish peroxidase) conjugated donkey anti-rabbit IgG antibody (ab16284, 1:5,000, Abcam) or donkey anti-mouse IgG antibody (Pierce) and visualized with the Pierce ECL Western Blotting substrate (Amersham), according to the provided protocol. Supplementary Figure 13 contains full scans of all Western blots.

For immunoprecipitation, 1 or 0.5 mg of protein extract was incubated overnight at 4°C with 10 μl Protein A or G beads (Life Technologies) preincubated for 2 hours at 4°C with 1 μg of BRD4 (ab128874, Abcam), MTHFD1 (A8, Santa Cruz) or GFP (G10362, Life Technology) antibodies.

Gene-Trap genetic screening

pGT-GFP contains an inactivated 3' LTR, a strong adenoviral (Ad40) splice-acceptor site, the GFP coding sequence and the SV40 polyadenylation signal. The Gene-trap virus was produced by transfection of 293T cells in T150 dishes with pGT-GFP combined with retroviral packaging plasmids. The virus-containing supernatant was collected after 30, 48 and 72 hours of transfection and concentrated using ultracentrifugation for 1.5 hours at 24,100 rpm in a Beckman Coulter Optima L-100 XP ultracentrifuge using an SW 32 Ti rotor.

For each replicate, 20 million REDS1 cells were mutagenized in a 24-well plate, seeding 1 million cells per well and using spin-infection for 45 minutes at 2,000 rpm. GT-infected cells were assessed by FACS to determine the percentage of infection (percentage of GFP-positive cells). If such percentage was above 70%, REDS1 GFP/RFP double-positive cells were sorted and left in culture for 2 weeks to get the sufficient number of cells to process for the DNA library preparation.

Gene-Trap analysis

Raw sequencing data were aligned to human reference genome hg19 (UCSC hg19 build) using bowtie2 (version 2.2.4) with default parameter. Reads that did not meet the following criteria were removed: (1) have a reported alignment - "mapped reads"; (2) have a unique alignment; (3) have a mapping quality (MAPQ) higher than 20. Duplicate reads were marked and discarded with Picard (version 1.111). Insertions in close proximity (1 or 2 base pairs distance from each other) were removed to avoid inclusion of insertions due to mapping errors. Insertions were annotated with gene build GRCh37.p13 (ENSEMBL 75 - release February 2014) using bedtools (version 2.10.1) and custom scripts. The canonical transcripts (according to ENSEMBL) for each gene were used as a reference gene model to count insertions falling with exons, introns or intragenic. Insertions were considered mutagenic or disruptive to the gene if they occurred within exons irrespective of their orientation to the corresponding gene or if they were located within introns in sense orientation[43]. Insertions in antisense direction in respect to the gene orientation were considered silent. All mutagenic insertions were summarized independently for each gene. For each gene a one-sided Fisher's exact test was applied to estimate a significant enrichment of insertions over an unselected control data set. Resulting *P* values were adjusted for false discovery rate (FDR) using Benjamini-Hochberg procedure. A cutoff of

Europe PMC Funders Author Manuscripts

5% FDR was considered significantly enriched. Insertion plots were drawn with R statistics software and Circos plots were produced using Circos[44].

DNA library preparation

DNA was extracted from 30 million GFP/RFP double-positive REDS1 cells using the Genomic DNA isolation QIAamp DNA mini kit (Qiagen). 4 μg of DNA were digested with NlaIII or MseI (4 digestions each enzyme). After spin column purification (Qiagen), 1 μg of digested DNA was ligated using T4 DNA ligase (NEB) in a volume of 300 μl (total of 4 ligations). The reaction mix was purified and retroviral insertion sites were identified via an inverse PCR protocol adapted to next-generation sequencing[45].

Immunopurification (IP-MS) and nanoLC-MS analysis

Anti-BRD4 (A301-985A, Bethyl Labs) antibody (50 μg) was coupled to 100 μl AminoLink resin (Thermo Fisher Scientific). Cell lysate samples (5 mg) were incubated with prewashed immuno-resin on a shaker for 2 hours at 4 °C. Beads were washed in lysis buffer containing 0.4% Igepal-CA630 and lysis buffer without detergent followed by two washing steps with 150 mM NaCl. Samples were processed by on-bead digest with Lys-C and Glycine protease before they were reduced, alkylated and digested with Trypsin.

The nano HPLC system used was an UltiMate 3000 HPLC RSLC nano system (Thermo Fisher Scientific, Amsterdam, Netherlands) coupled to a Q Exactive mass spectrometer (Thermo Fisher Scientific, Bremen, Germany), equipped with a Proxeon nanospray source (Thermo Fisher Scientific, Odense, Denmark).

The Q Exactive mass spectrometer was operated in data-dependent mode, using a full scan (m/z range 350-1650, nominal resolution of 70,000, target value 1E6) followed by MS/MS scans of the 12 most abundant ions. MS/MS spectra were acquired using normalized collision energy 30%, isolation width of 2 and the target value was set to 5E4. Precursor ions selected for fragmentation (charge state 2 and higher) were put on a dynamic exclusion list for 30 s. Additionally, the underfill ratio was set to 20% resulting in an intensity threshold of 2E4. The peptide match feature and the exclude isotopes feature were enabled.

Generation of MTHFD1 KO HAP1cell lines

To generate MTHFD1 knock-out (KO) mutants, guide RNAs (gRNAs) were designed using the CRISPR Design Tool (http://tools.genome-engineering.org) and cloned into pSpCas9(BB)-2A-Puro (PX459) V2.0 (Addgene plasmid # 62988, a gift from Dr. Feng Zhang)[46]. HAP1 cells were transiently transfected with PX459 containing the gRNAs by using TurboFectin (OriGene) according to manufacturer's instructions. Transfected cells were under puromycin selection for 2 days, afterwards the resistant cells were at a low density for single clones picking. KO clones were verified by both PCR reaction and western blot.

Europe PMC Funders Author Manuscripts

Generation of MTHFD1 NES and NLS vectors

The MTHFD1 consensus coding sequence was previously inserted into pcDNA3_N-DYK by gene synthesis (GenScript) to generate MTHFD1 complementary plasmid (MTHFD1-WT, pcDNA3_N-DYK-MTHFD1).

To generate pcDNA3_N-DYK_MTHFD1-NES (Nuclear Export Signal) and pcDNA3_N-DYK_MTHFD1-NLS (Nuclear Localization Signal) plasmids, NES/NLS sequences were fused to MTHFD1-WT through site-directed mutagenesis (NEB) according to user's manual.

Preparation of nuclear cell extracts for metabolomics

Nuclei were extracted by hypotonic lysis. Briefly, intact cells treated (as indicated in the results section) were washed twice with cold PBS and incubated on ice for 10 minutes with hypotonic lysis buffer (10 mM HEPES, pH 7.9, with 1.5 mM $MgCl_2$, 10 mM KCl and protease inhibitor cocktail (cOmplete, Roche); buffer-cells volume ratio 5:1). Pellet was gently resuspended three times during the incubation. Nuclei were collected by centrifugation (420 g × 5 minutes) and immediately snap frozen.

The metabolomic assay and data analysis was performed by Metabolomic Discoveries (http://www.metabolomicdiscoveries.com; Germany). Briefly, LC-QTOF/MS-based non-targeted metabolite profiling was used to analyses nuclear metabolites in the range of 50-1,700 Da, with an accuracy up to 1-2 ppm and a resolution of mass/Δmass=40.000. Metabolites measured in the LC are annotated according to their accurate mass and subsequent sum formula prediction. Metabolites that were not annotated in the LC-MS-analyses are listed according to their accurate mass and retention time.

Folate extraction for LC MS/MS analysis

In order to quantify folates in the nuclear and cytosolic fractions, 20 million HAP1 cells per condition were washed twice with cold PBS, and collected into 50 ml Falcon tube by centrifugation for 5 minutes at 280 g and 4 °C. Cell lysis was performed on ice in the dark by incubating cell pellets with 1:5 hypotonic lysis buffer for 10 minutes. Nuclei were collected by centrifugation for 5 minutes at 420 g and 4 °C. Supernatants (cytosolic fractions) were also collected. Both fractions were immediately snap frozen.

For nucleus samples, 10 µl of ISTD mixture was added to nucleus pellet in 1.5 ml Eppendorf tube followed by addition of 145 µl of ice-cold extraction solvent (10 mg/ml ascorbic acid solution in 80% methanol, 20% water, v/v). The samples were vortexed for 10 seconds, afterwards incubated on ice for 3 min and vortexed again for 10 seconds. After centrifugation (14,000 rpm, 10 min, 4 °C), the supernatant was collected into HPLC vials. The extraction step was repeated and combined supernatants were used for LC-MS/MS analysis.

For cytoplasm samples, 10 µl of ISTD mixture was added to 75 µl of cytoplasm 1.5 ml Eppendorf tube followed by addition of 215 µl of ice-cold extraction solvent (10 mg/ml ascorbic acid solution in 80% methanol, 20% water, v/v). The samples were vortexed for 10 seconds, afterwards incubated on ice for 3 min and vortexed again for 10 seconds. After

centrifugation (14,000 rpm, 10 min, 4 °C), the supernatant was collected into HPLC vials and used for LC-MS/MS analysis.

LC MS/MS analysis of folates

An Acquity UHPLC system (Waters) coupled with Xevo TQ-MS (Waters) triple quadrupole mass spectrometer was used for quantitative analysis of metabolites. The separation was conducted on an ACQUITY HSS T3, 1.8 μm, 2.1 × 100 mm column (Waters) equipped with an Acquity HSS T3 1.8 μM Vanguard guard column (Waters) at 40 °C. The separation was carried out using 0.1% formic acid (v/v) in water as a mobile phase A, and 0.1% formic acid (v/v) in methanol as a mobile phase B. The gradient elution with a flow rate 0.5 ml/min was performed with a total analysis time of 10 min. The autosampler temperature was set to 4 °C. For detection, Waters Xevo TQ-MS in positive electrospray ionization mode with multiple reaction mode was employed. Quantification of all metabolites was performed using MassLynx V4.1 software from Waters. The seven point linear calibration curves with internal standardization and 1/x weighing was constructed for the quantification.

^{13}C-formate sample preparation and ^{13}C tracing analysis of nucleotides by LC-MS

HAP1 WT and MTHFD1 KO cells were seeded at 350.000 cells/ml in media containing 1 mM of ^{13}C-formate (Cambridge Isotope Laboratories, Inc. (CDLM-6203-0.5)) for 24 hours. Following the incubation, RNA was extracted using the RNeasy Mini Kit (Qiagen (74106)) and 2 μg of RNA were hydrolyzed to single nucleotides (alkaline hydrolysis) with 0.3 N NaOH for 16 hours at 37 °C, shaking (300 rpm). 0.3 N HCl was added to neutralize the alkaline pH. For the LC-MS analysis, 40 μl of methanol was added to 10 μl of hydrolzed RNA solution. The samples were vortexed for 10 seconds, centrifuged (14,000 rpm, 5 min, 4 °C), and the supernatant was transferred into HPLC vial. A Vanquish UHPLC system (Thermo) coupled with Orbitrap Fusion Lumos Tribrid (Thermo) mass spectrometer was used for the ^{13}C tracing analysis of nucleotides. The separation was carried out on an ACQUITY UPLC BEH Amide, 1.7 μm, 2.1 × 100 mm analytical column (Waters) equipped with Waters VanGuard: BEH C18, 2.1 × 5 mm pre-column. The gradient elution using 0.15% formic acid (v/v) in water as mobile phase A and 0.15% formic acid (v/v) in 85% acetonitrile (v/v) with 10 mM ammonium formate as mobile phase B was applied. For detection, Orbitrap Fusion Lumos (Thermo) in positive ionization mode was employed. Acquisition of isotopologue distribution was done using the Orbitrap MS scan with the resolution 500,000, scan range from 110 m/z to 500 m/z, AGC target of 2.0 e5, and maximum injection time of 50 ms. TraceFinder software (Thermo) was employed for the data processing.

ChIP-seq sample preparation

Three 15 cm dishes with cells at 70-80 % of confluency were used for one ChIP experiment. Briefly, cells were cross-linked with 1% formaldehyde for 10 minutes at room temperature, and then quenched with 125 mM glycine for 5 minutes at room temperature. Then, cells were washed with cold PBS, collected in 15 ml tubes and washed again with cold PBS by centrifugation at 1,200 rpm for 5 minutes at 4 °C and finally snap-frozen.

Europe PMC Funders Author Manuscripts

ChIP was performed as described[47] by using BRD4 (Bethyl Laboratories, Inc.) and MTHFD1 (sc-271413, Santa Cruz) antibodies. In brief, crosslinked cell lysates were sonicated in order to shred the chromatin into 200-500 bp fragments. Fragmented chromatin was incubated overnight at 4 °C with antibodies, followed by 2 hours at 4 °C with pre-blocked Dynabeads Protein G (ThermoFisher Scientific). Beads were washed twice with low salt buffer, twice with high salt buffer, twice with LiCl buffer, twice with 1× TE buffer and finally eluted with elution buffer for 20 min at 65 °C. The elution products were treated with RNaseA for 30 minutes at 37 °C, followed by proteinase K treatment at 55 °C for 1 hour, and then incubated at 65 °C overnight to reverse the crosslinks. The samples were further purified by using a PCR purification kit (Qiagen). ChIP-seq libraries were sequenced by the Biomedical Sequencing Facility at CeMM using the Illumina HiSeq3000/4000 platform and the 50-bp single-end configuration.

ChIP-seq and RNA-seq data analysis

Next-generation sequencing libraries were sequenced by the Biomedical Sequencing Facility at CeMM using the Illumina HiSeq3000/4000 platform and the 50-bp single-end configuration. For ChIP-seq, reads containing adapters were trimmed using Skewer[48] and aligned to the hg19/GRCh37 assembly of the Human genome using Bowtie2[49] with the "--very-sensitive" parameter and duplicate reads were marked and removed with sambamba. Library quality was assessed with the phantomPeakQualtools scripts[50]. We used HOMER findPeaks[51] to call peaks on both replicates with matched IgG controls as background. This was done in in "factor" mode for BRD4 and in "histone" mode for MTHFD1. We used GREAT[52] to assign regions to putative regulated genes with default parameters and to retrieve enriched gene functions from BRD4- or MTHFD1-bound regions. For visualization, we generated genome browser tracks with deeptools2[53] using RPGC normalization (reads per bin scaled to 1× genome coverage) which were also input to generate visualizations of ChIP-seq signal in peaks either for each peak or in aggregate. This was done for each sample individually and for replicates merged. DiffBind[54] was used to detect differential binding of BRD4 or MTHFD1 in a consensus set of bound regions by the two factors, for MTHFD1 KO or dBET6-treated samples against the respective controls. Regions with absolute $\log_2$ fold-change higher than 1 and FDR-adjusted P value smaller than 0.1 were used to display ChIP-seq intensity values using the estimated concentration values from DiffBind. Total differences between ChIP-seq levels in these regions between conditions were tested with a Mann-Whitney U test. For RNA-seq data, we used RPKM values as estimated by the Cufflinks software suite[55] and employed limma removeBatchEffect function to integrate datasets produced in different batches with default parameters. Genes associated with diferentially bound sites by BRD4 or MTHFD1 as retrieved from GREAT were used to display distributions of $\log_2$ fold-changes of expression as estimated by the Cufflinks links for RNA-seq data. Overlap between bound genes and differentially expressed genes was tested with a Fisher's exact test and the P values were corrected with the FDR method. We make all epigenomic data (GEO accession GSE105786) and data analysis code (https://github.com/epigen/mthfd1) available.

Mouse xenograft studies

Mouse xenograft studies were performed as described previously[27]. 2×10^6 A549 cells, diluted 1:1 in matrigel, were transplanted subcutaneously into NOD SCID gamma mice. Treatment (30 mg/kg (*S*)-JQ1 by intraperitoneal injection five times per week, and 25 mg/kg MTX per intraperitoneal injection twice weekly) was started when tumors were established, 19 days post transplantation. Tumor volumes were evaluated twice a week by measuring two perpendicular diameters with calipers. Tumor volume was calculated using the following equation: (width*width*length)/2. Treatment was performed according to an animal license protocol approved by the Bundesministerium für Wissenschaft und Forschung (BMWF-66.009/0280-II/3b/2012). At day 43, mice were sacrificed and tumors excised and weighted.

Statistics

Statistical tests used are described in the respective figure legends and methods sections.

The following panels are representative of experiments repeated the following number of times: Fig. 1c - triplicate, Fig. 1d – triplicate, Fig. 1e – duplicate, Fig. 2b – duplicate, Fig. 2c – triplicate, Fig. 2d – triplicate, Fig. 2e – duplicate, Fig. 2f – duplicate, Fig. 3a – triplicate, Fig. 4b – duplicate.

Supplementary Material

Refer to Web version on PubMed Central for supplementary material.

Acknowledgements

S.S. is a JDRF postdoctoral fellow (3-PDF-2014-206-A-N). D.L.B. is a Merck Fellow of the Damon Runyon Cancer Research Foundation (DRG-2196-14). Next-generation sequencing was performed by the Biomedical Sequencing Facility at CeMM. Research in the Kubicek laboratory is supported by the Austrian Federal Ministry for Digital and Economic Affairs and the National Foundation for Research, Technology, and Development, the Austrian Science Fund (FWF) F4701 and the European Research Council (ERC) under the European Union's Horizon 2020 research and innovation programme (ERC-CoG-772437). Research in the Zuber laboratory was supported by the European Research Council (ERC-StG-336860; to J.Z.), a Research Fellowship of the E.U. (Marie Curie Actions; to P.R.), and generous institutional funding from Boehringer Ingelheim. We thank all the members of the BioOptic Facility of the Research Institute of Molecular Pathology (IMP) and the Institute of Molecular Biotechnology GmbH (IMBA) for their help with cell sorting, Patrick Stover (Cornell) and Sebastian Nijman (Oxford) for kindly providing plasmids, and Alessio Terenzi (DIPC) for his advice on *in vitro* metabolomics.

References

1. Filippakopoulos P, et al. Histone recognition and large-scale structural analysis of the human bromodomain family. Cell. 2012; 149:214–31. [PubMed: 22464331]
2. Floyd SR, et al. The bromodomain protein Brd4 insulates chromatin from DNA damage signalling. Nature. 2013; 498:246–50. [PubMed: 23728299]
3. Filippakopoulos P, et al. Selective inhibition of BET bromodomains. Nature. 2010; 468:1067–73. [PubMed: 20871596]
4. Winter GE, et al. BET Bromodomain Proteins Function as Master Transcription Elongation Factors Independent of CDK9 Recruitment. Mol Cell. 2017; 67:5–18 e19. [PubMed: 28673542]
5. Shi J, Vakoc CR. The mechanisms behind the therapeutic activity of BET bromodomain inhibition. Mol Cell. 2014; 54:728–36. [PubMed: 24905006]

6. Zhou Q, Li T, Price DH. RNA polymerase II elongation control. Annu Rev Biochem. 2012; 81:119–43. [PubMed: 22404626]
7. Asangani IA, et al. Therapeutic targeting of BET bromodomain proteins in castration-resistant prostate cancer. Nature. 2014; 510:278–82. [PubMed: 24759320]
8. Dawson MA, et al. Inhibition of BET recruitment to chromatin as an effective treatment for MLL-fusion leukaemia. Nature. 2011; 478:529–33. [PubMed: 21964340]
9. Delmore JE, et al. BET bromodomain inhibition as a therapeutic strategy to target c-Myc. Cell. 2011; 146:904–17. [PubMed: 21889194]
10. Loven J, et al. Selective inhibition of tumor oncogenes by disruption of super-enhancers. Cell. 2013; 153:320–34. [PubMed: 23582323]
11. Shu S, et al. Response and resistance to BET bromodomain inhibitors in triple-negative breast cancer. Nature. 2016; 529:413–7. [PubMed: 26735014]
12. Zuber J, et al. RNAi screen identifies Brd4 as a therapeutic target in acute myeloid leukaemia. Nature. 2011; 478:524–8. [PubMed: 21814200]
13. Filippakopoulos P, Knapp S. Targeting bromodomains: epigenetic readers of lysine acetylation. Nat Rev Drug Discov. 2014; 13:337–56. [PubMed: 24751816]
14. Knoechel B, et al. An epigenetic mechanism of resistance to targeted therapy in T cell acute lymphoblastic leukemia. Nat Genet. 2014; 46:364–70. [PubMed: 24584072]
15. Rathert P, et al. Transcriptional plasticity promotes primary and acquired resistance to BET inhibition. Nature. 2015; 525:543–7. [PubMed: 26367798]
16. Fong CY, et al. BET inhibitor resistance emerges from leukaemia stem cells. Nature. 2015; 525:538–42. [PubMed: 26367796]
17. Sdelci S, et al. Mapping the chemical chromatin reactivation landscape identifies BRD4-TAF1 cross-talk. Nat Chem Biol. 2016; 12:504–10. [PubMed: 27159579]
18. Carette JE, et al. Haploid genetic screens in human cells identify host factors used by pathogens. Science. 2009; 326:1231–5. [PubMed: 19965467]
19. Tchasovnikarova IA, et al. GENE SILENCING. Epigenetic silencing by the HUSH complex mediates position-effect variegation in human cells. Science. 2015; 348:1481–5. [PubMed: 26022416]
20. Sabari BR, et al. Coactivator condensation at super-enhancers links phase separation and gene control. Science. 2018; 361
21. Cho WK, et al. Mediator and RNA polymerase II clusters associate in transcription-dependent condensates. Science. 2018; 361:412–415. [PubMed: 29930094]
22. Ducker GS, Rabinowitz JD. One-Carbon Metabolism in Health and Disease. Cell Metab. 2016
23. Field MS, et al. Nuclear enrichment of folate cofactors and methylenetetrahydrofolate dehydrogenase 1 (MTHFD1) protect de novo thymidylate biosynthesis during folate deficiency. J Biol Chem. 2014; 289:29642–50. [PubMed: 25213861]
24. Field MS, Kamynina E, Stover PJ. MTHFD1 regulates nuclear de novo thymidylate biosynthesis and genome stability. Biochimie. 2016; 126:27–30. [PubMed: 26853819]
25. Winter GE, et al. DRUG DEVELOPMENT. Phthalimide conjugation as a strategy for in vivo target protein degradation. Science. 2015; 348:1376–81. [PubMed: 25999370]
26. Bliss CI. The toxicity of poisons applied jointly. Ann Appl Biol. 1939; 26:585–615.
27. Grabner B, et al. Disruption of STAT3 signalling promotes KRAS-induced lung tumorigenesis. Nat Commun. 2015; 6:6285. [PubMed: 25734337]
28. Wright RH, et al. ADP-ribose-derived nuclear ATP synthesis by NUDIX5 is required for chromatin remodeling. Science. 2016; 352:1221–5. [PubMed: 27257257]
29. Mews P, et al. Acetyl-CoA synthetase regulates histone acetylation and hippocampal memory. Nature. 2017; 546:381–386. [PubMed: 28562591]
30. Kamynina E, et al. Arsenic trioxide targets MTHFD1 and SUMO-dependent nuclear de novo thymidylate biosynthesis. Proc Natl Acad Sci U S A. 2017; 114:E2319–E2326. [PubMed: 28265077]
31. MacFarlane AJ, et al. Nuclear localization of de novo thymidylate biosynthesis pathway is required to prevent uracil accumulation in DNA. J Biol Chem. 2011; 286:44015–22. [PubMed: 22057276]

32. Field MS, Kamynina E, Chon J, Stover PJ. Nuclear Folate Metabolism. Annu Rev Nutr. 2018; 38:219–243. [PubMed: 30130467]
33. Ginno PA, Burger L, Seebacher J, Iesmantavicius V, Schubeler D. Cell cycle-resolved chromatin proteomics reveals the extent of mitotic preservation of the genomic regulatory landscape. Nat Commun. 2018; 9:4048. [PubMed: 30279501]
34. Sudhamalla B, Dey D, Breski M, Nguyen T, Islam K. Site-specific azide-acetyllysine photochemistry on epigenetic readers for interactome profiling. Chem Sci. 2017; 8:4250–4256. [PubMed: 28626565]
35. Perretta M, Romero A. De novo RNA biosynthesis in isolated bone marrow nuclei. Experientia. 1973; 29:39–40. [PubMed: 4729447]
36. Tan JL, et al. Stress from Nucleotide Depletion Activates the Transcriptional Regulator HEXIM1 to Suppress Melanoma. Mol Cell. 2016; 62:34–46. [PubMed: 27058786]
37. Sharma U, Rando OJ. Metabolic Inputs into the Epigenome. Cell Metab. 2017; 25:544–558. [PubMed: 28273477]
38. Li X, Egervari G, Wang Y, Berger SL, Lu Z. Regulation of chromatin and gene expression by metabolic enzymes and metabolites. Nat Rev Mol Cell Biol. 2018; 19:563–578. [PubMed: 29930302]
39. Boukouris AE, Zervopoulos SD, Michelakis ED. Metabolic Enzymes Moonlighting in the Nucleus: Metabolic Regulation of Gene Transcription. Trends Biochem Sci. 2016; 41:712–730. [PubMed: 27345518]
40. van der Knaap JA, Verrijzer CP. Undercover: gene control by metabolites and metabolic enzymes. Genes Dev. 2016; 30:2345–2369. [PubMed: 27881599]
41. Anderson AC, Wright DL. Antifolate agents: a patent review (2010 - 2013). Expert Opin Ther Pat. 2014; 24:687–97. [PubMed: 24655343]
42. Wilson PM, Danenberg PV, Johnston PG, Lenz HJ, Ladner RD. Standing the test of time: targeting thymidylate biosynthesis in cancer therapy. Nat Rev Clin Oncol. 2014; 11:282–98. [PubMed: 24732946]
43. Burckstummer T, et al. A reversible gene trap collection empowers haploid genetics in human cells. Nat Methods. 2013; 10:965–71. [PubMed: 24161985]
44. Krzywinski M, et al. Circos: an information aesthetic for comparative genomics. Genome Res. 2009; 19:1639–45. [PubMed: 19541911]
45. Carette JE, et al. Global gene disruption in human cells to assign genes to phenotypes by deep sequencing. Nat Biotechnol. 2011; 29:542–6. [PubMed: 21623355]
46. Ran FA, et al. Genome engineering using the CRISPR-Cas9 system. Nat Protoc. 2013; 8:2281–2308. [PubMed: 24157548]
47. Kim TH, et al. A high-resolution map of active promoters in the human genome. Nature. 2005; 436:876–80. [PubMed: 15988478]
48. Jiang H, Lei R, Ding SW, Zhu S. Skewer: a fast and accurate adapter trimmer for next-generation sequencing paired-end reads. BMC Bioinformatics. 2014; 15:182. [PubMed: 24925680]
49. Langmead B, Salzberg SL. Fast gapped-read alignment with Bowtie 2. Nat Methods. 2012; 9:357–9. [PubMed: 22388286]
50. Landt SG, et al. ChIP-seq guidelines and practices of the ENCODE and modENCODE consortia. Genome Res. 2012; 22:1813–31. [PubMed: 22955991]
51. Heinz S, et al. Simple combinations of lineage-determining transcription factors prime cis-regulatory elements required for macrophage and B cell identities. Mol Cell. 2010; 38:576–89. [PubMed: 20513432]
52. McLean CY, et al. GREAT improves functional interpretation of cis-regulatory regions. Nat Biotechnol. 2010; 28:495–501. [PubMed: 20436461]
53. Ramirez F, et al. deepTools2: a next generation web server for deep-sequencing data analysis. Nucleic Acids Res. 2016; 44:W160–5. [PubMed: 27079975]
54. Ross-Innes CS, et al. Differential oestrogen receptor binding is associated with clinical outcome in breast cancer. Nature. 2012; 481:389–93. [PubMed: 22217937]

55. Trapnell C, et al. Transcript assembly and quantification by RNA-Seq reveals unannotated transcripts and isoform switching during cell differentiation. Nat Biotechnol. 2010; 28:511–5. [PubMed: 20436464]

Europe PMC Funders Author Manuscripts

Europe PMC Funders Author Manuscripts

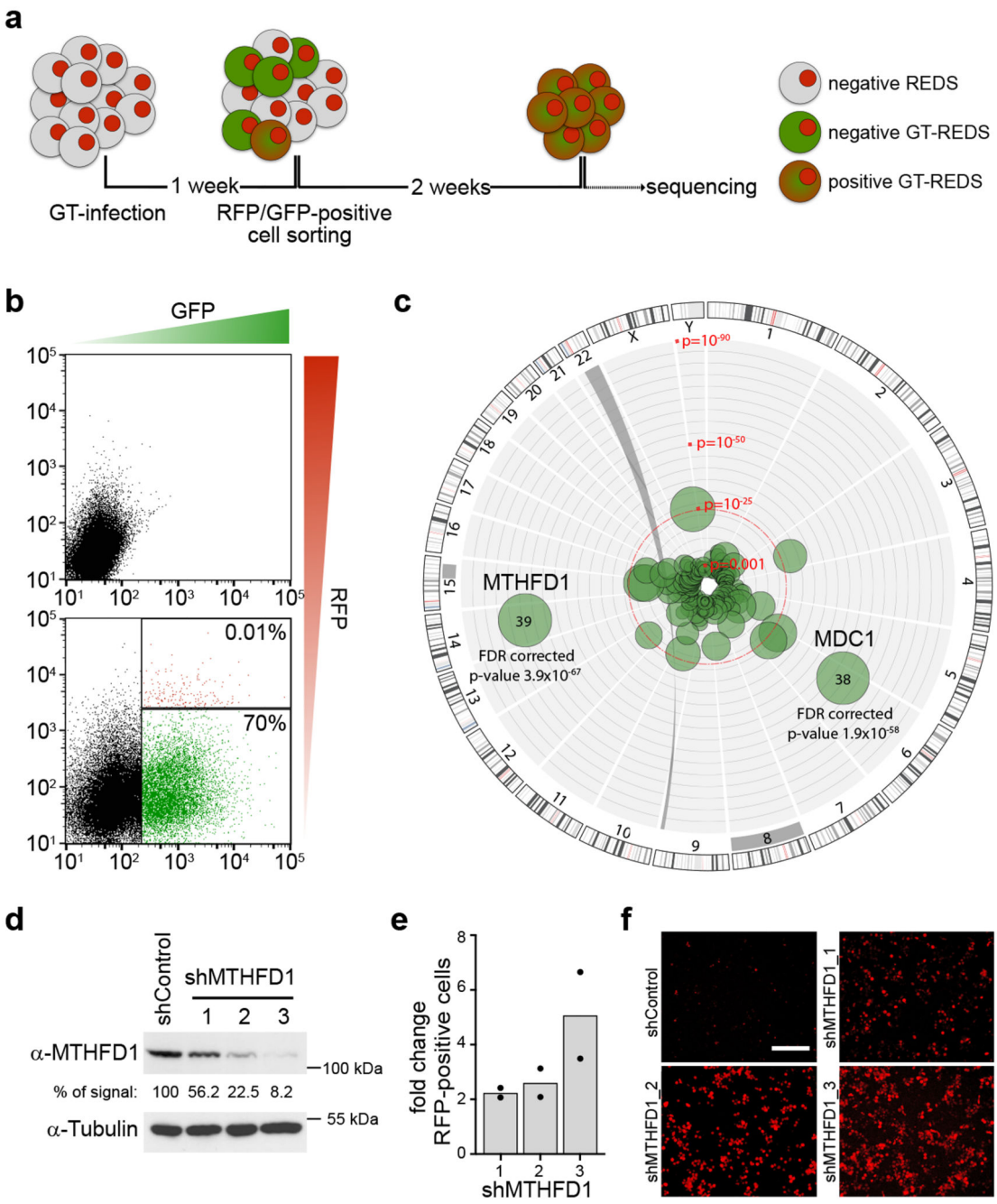

Figure 1. A genetic screen identifies MTHFD1 as a functional partner of BRD4.

a, Schematic overview of the gene-trap based genetic screen. **b**, Representative panels of the applied FACS-sorting strategy showing non-infected (upper panel) and gene-trap infected (lower panel) REDS1 cells; infected double-positive (GFP^+/RFP^+) cells (shown in red: 0.01%) were sorted. **c**, Circos plot illustrating the results from the gene-trap screen by genomic location (outside ring), number of independent inactivating integrations (bubble size) and significance (distance from center). *P* values were calculated by one-sided Fisher's exact test of insertions over an unselected control data set adjusted for false discovery rate

(FDR) using Benjamini-Hochberg procedure. The screen was performed in three biologically independent experiments. **d**, Western blot showing MTHFD1 protein levels after downregulation with the indicated shRNAs in REDS1 cells. Numbers indicate the percentage of MTHFD1 protein remaining, tubulin was used as a loading control. The experiment was repeated three times with similar results. **e**, Quantification of RFP^+ cells from live-cell imaging of REDS1 cells treated with MTHFD1 shRNA. Two biological replicates were done for each experimental condition. **f**, Representative live-cell images of MTHFD1 knock-down in REDS1 cells. Scale bar 100 μm.

Europe PMC Funders Author Manuscripts

Europe PMC Funders Author Manuscripts

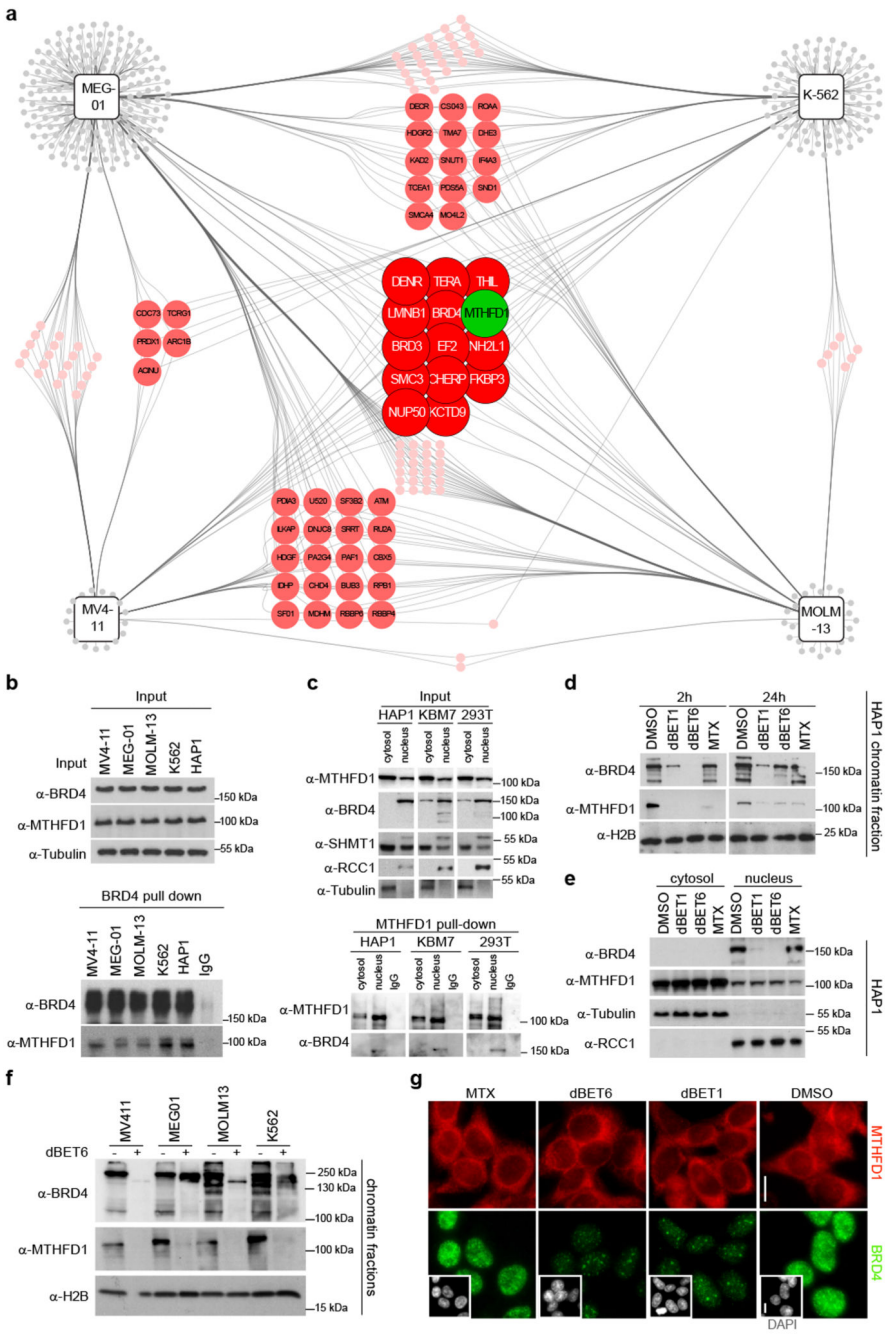

Figure 2. BRD4 recruits MTHFD1 to chromatin.

a, BRD4 interactomes in MEG-01, K-562, MV4-11and MOLM-13 cell lines. Proteins are represented as circles, colors indicate the number of cell lines in which a particular interacting protein was detected. **b**, Western blot confirmation of the BRD4-MTHFD1 interaction in leukemia cell lines. The experiment was repeated twice with similar results. **c**, Upper panel: Western blot following nuclear *vs* cytoplasmic fractionation in HAP1, KBM7 and HEK293T cell lines. RCC1 was used as nuclear loading control while tubulin was used as cytosolic loading control. Lower panel: Western blot following MTHFD1 pull-down in

the different cell fractions. The experiment was repeated three times with similar results. **d**, Western blot performed on chromatin-associated protein samples extracted from HAP1 cells treated with the indicated compounds for 2 h (dBET1: 0.5 μM; dBET6: 0.5 μM; MTX: 1 μM) or 24 h (dBET1: 0.5 μM; dBET6: 0.05 μM; MTX: 1 μM). H2B was used as loading control. The experiment was repeated three times with similar results. **e**, Western blot for nuclear *vs* cytoplasmic protein levels in HAP1 cells treated for 24 h as above. The experiment was repeated twice with similar results. **f**, Western blot from chromatin fractions of MEG-01, K-562, MV4-11 and MOLM-13 cells treated with dBET6 for 2 h. The experiment was repeated twice with similar results. **g**, Immunofluorescence images of HeLa cells treated with the indicated compounds and stained for MTHFD1, BRD4, and DAPI (small inserts). Scale bar 10 μm.

Europe PMC Funders Author Manuscripts

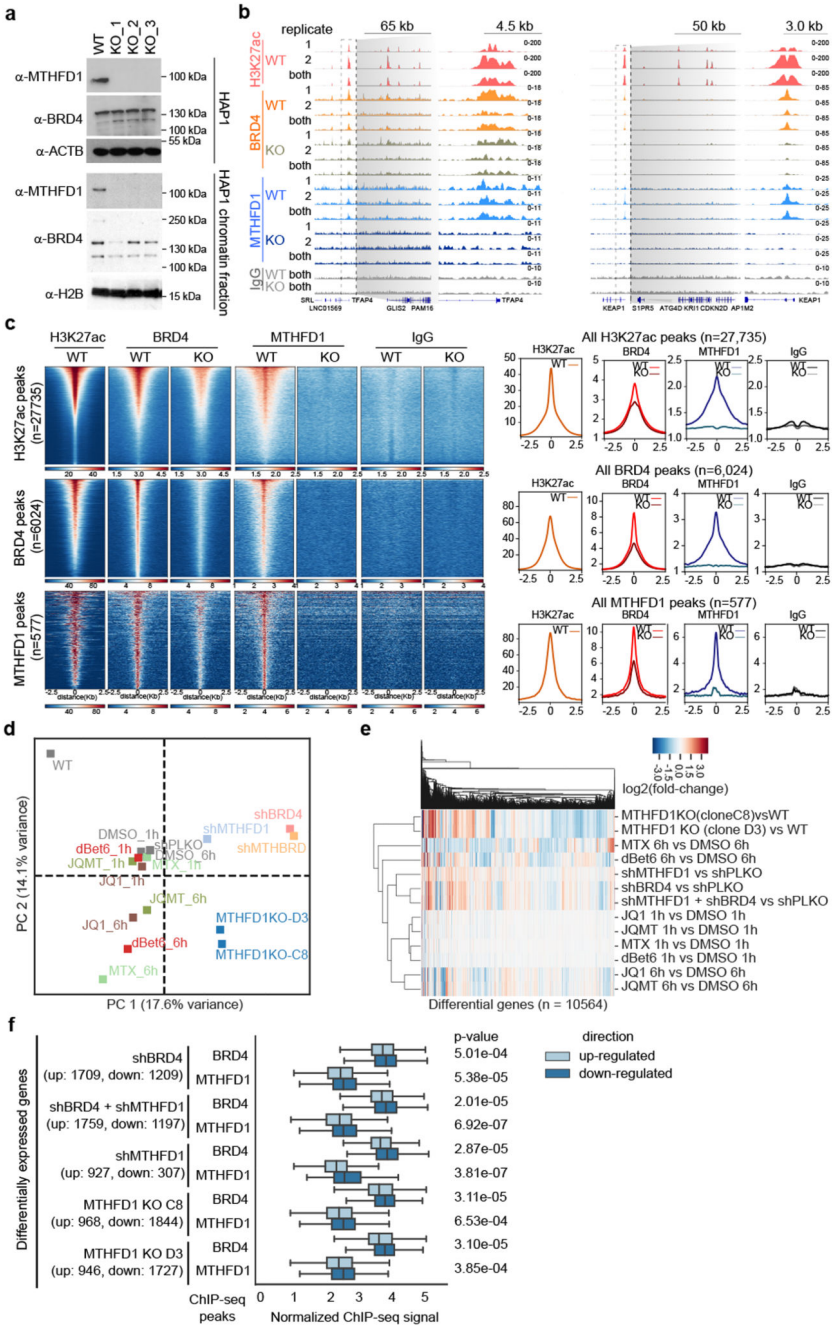

Figure 3. MTHFD1 regulates transcription by binding BRD4-occupied chromatin.

a, Validation of MTHFD1 knock-out HAP1 cell lines. The experiment was repeated three times with similar results. **b**, Representative genome browser view of BRD4, MTHFD1, and H3K27ac binding in the promoters of TFAP4 (left) and KEAP1 (right). All ChIP tracks were normalized to 1X genome coverage. All the IPs were performed in biological duplicate. Specifically for MTHFD1 knock-out cells, MTHFD1 KO_1 and MTHFD1 KO_3 were used as independent biological replicates. **c**, Enrichment of BRD4 and MTHFD1 ChIP signal. Peaks were sorted by total abundance and data represent merged replicates normalized to 1×

Europe PMC Funders Author Manuscripts

coverage. **d**, Principal component analysis of RNA-seq data of two MTHFD1 knock-out clones and of WT HAP1 cells treated with 0.1 μM dBET6, 1 μM (*S*)-JQ1, 1 μM MTX, shRNAs targeting BRD4 or MTHFD1. Equal amount of DMSO, or non-targeting hairpins were used as respective control conditions and two biological replicates were performed for each experimental condition. **e**, Heatmap of relative transcription changes in HAP1 cells compared to respective control cells. **f**, Integration of ChIP-seq and RNA-seq data in HAP1 cells. BRD4 and MTHFD1 binding at sites associated with genes which are significantly up- or down-regulated upon knockdown of BRD4 and/or MTHFD1 and in MTHFD1 knock-out cells compared to HAP1 WT cells. Values represent estimated factor abundance normalized by matched IgG signal and equality of distributions was assessed with with a one-sided Mann–Whitney U test. Boxplot boxes represent interquartile range with center on median, and whiskers represent values 1.5× outside the respective interquartile range.

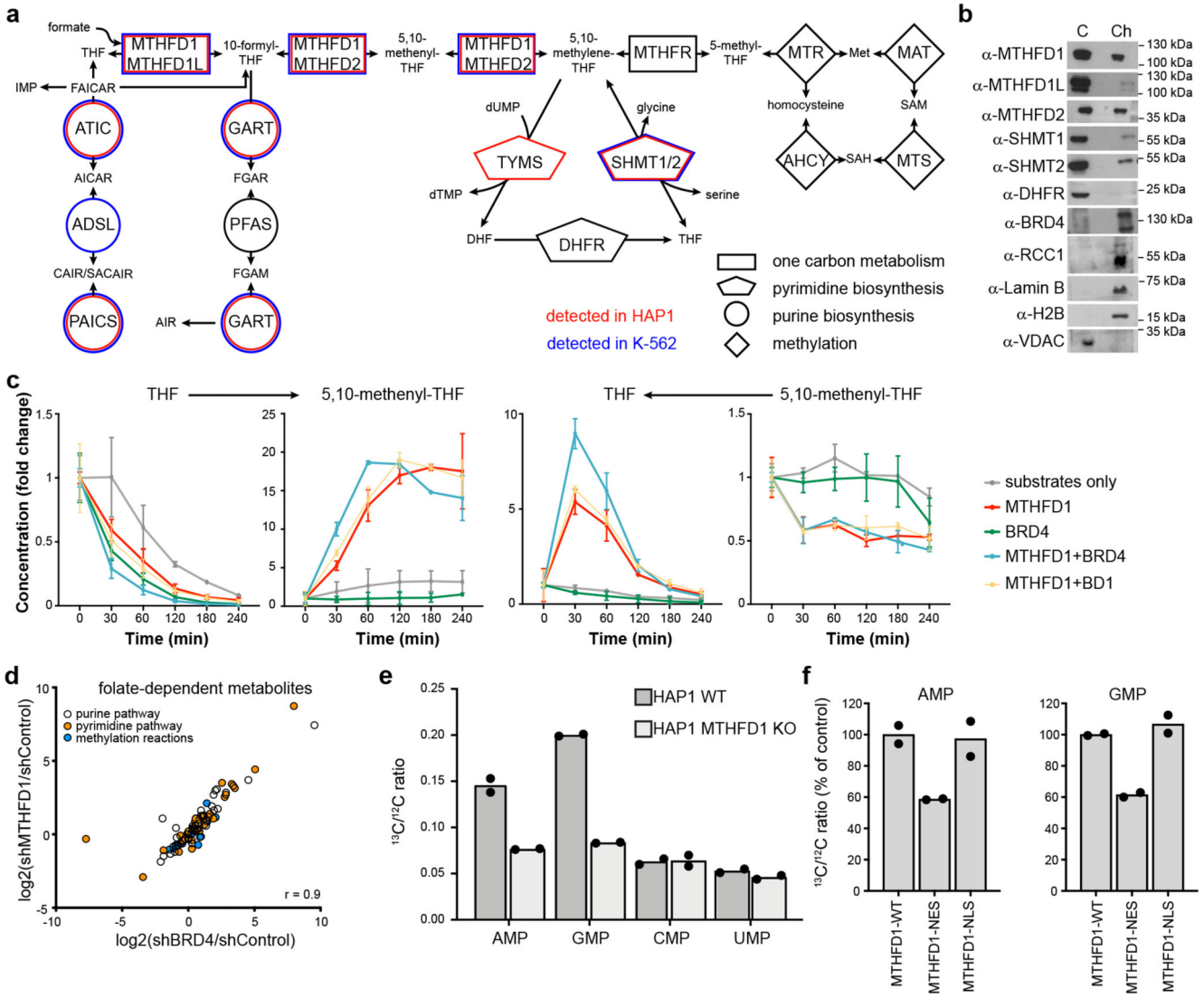

Figure 4. Effects of MTHFD1 loss on nuclear metabolite composition.

a, Representation of the folate pathway. Enzyme names are reported inside the geometric shapes, connecting the different metabolites. Enzymes that were found associated with chromatin in HAP1 and K-562 cells by mass spectrometry analysis are indicated in red and blue, respectively. Two biological replicates were done. **b**, Western blot for folate pathway enzymes in the cytoplasmic (C) and chromatin (Ch) fractions of HAP1 cells. The experiment was repeated twice with similar results. **c**, Recombinant enzyme assays for MTHFD1 activity to convert THF and formate to 5,10-methenyl-THF and vice versa in the presence or absence of full-length BRD4 or its first bromodomain. Mean ± SD from n = 2 independent samples. **d**, Scatter plot representing metabolite changes in the pyrimidine, purine and methionine biosynthetic pathways upon downregulation of BRD4 or MTHFD1 by shRNA. Two biological replicates were done for each experimental condition. *r*-value indicates the Pearson correlation coefficient. **e**, Incorporation of labeled formate into RNA. HAP1 WT and MTHFD1 knock-out cells were treated with ^{13}C-labeled formate for 24 h, followed by

Europe PMC Funders Author Manuscripts

RNA extraction and LC-MS-MS analysis of nucleotides for the $^{13}C/^{12}C$ ratio. Two biological replicates were performed for each experimental condition. **f**, Incorporation of labeled formate into RNA using the same procedure with MTHFD1 knock-out cells transiently transfected with full-length MTHFD1, or the protein with either a nuclear localization signal (NLS) or a nuclear export signal (NES). Percent of control is calculated considering the ^{13}C incorporation in HAP1 WT and MTHFD1 knock-out respectively as 100% and 0. Two biological replicates were performed for each experimental condition.

Europe PMC Funders Author Manuscripts

Europe PMC Funders Author Manuscripts

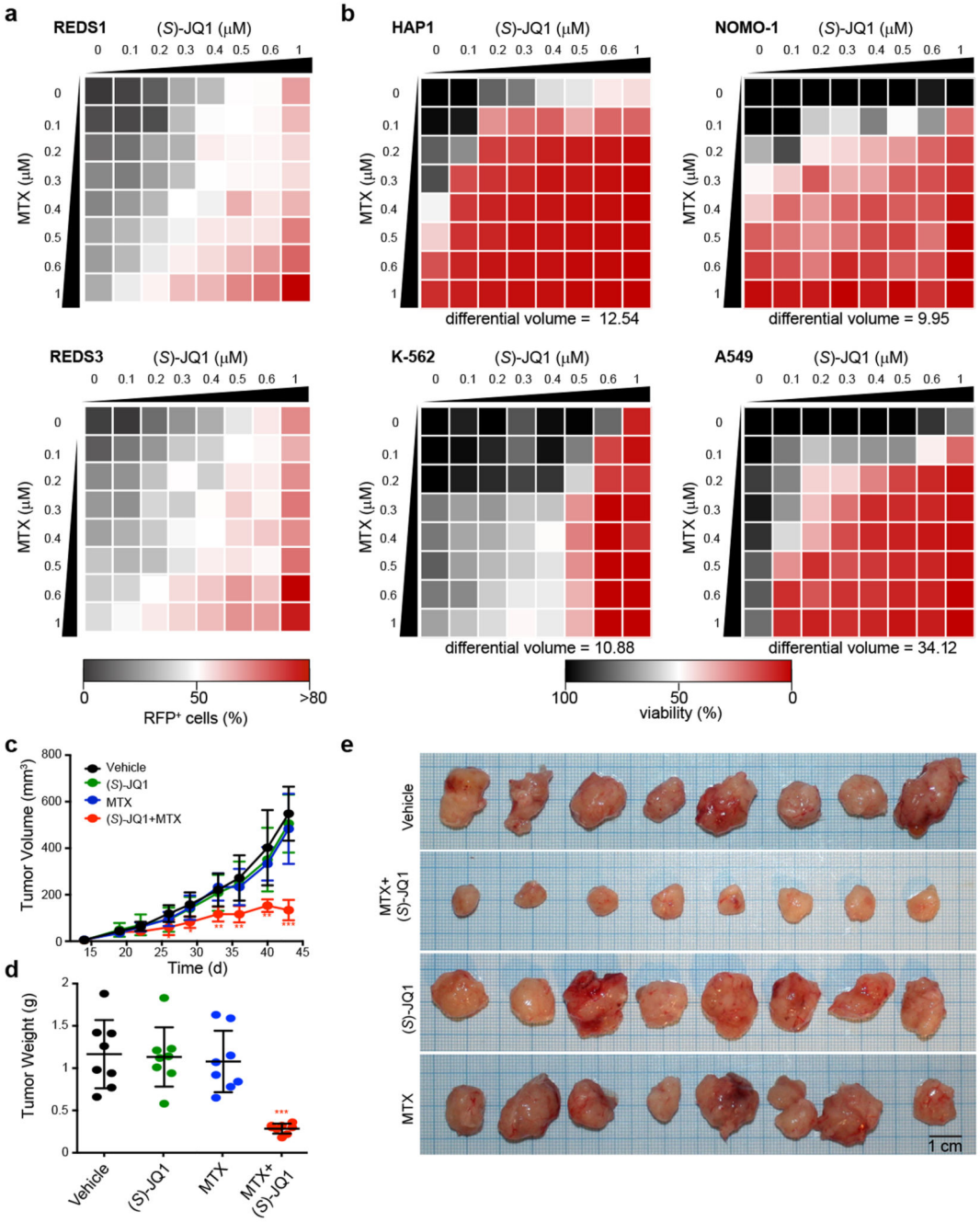

Figure 5. BET bromodomain inhibitors synergize with antifolates to impair cancer cell growth.

a, Dose response matrix displaying REDS1 and REDS3 RFP-positive cells treated with the indicated concentrations of (S)-JQ1 and MTX alone or in combination. Means from two biological replicates. **b**, Dose response matrices displaying cell viability of HAP1, NOMO-1, K-562 and A549 treated for 72 h with (*S*)-JQ1 and MTX alone or in combination. Means from two biological replicates. Differential volume indicates the sum of all deviations from Bliss additivity over the dose response matrix. **c**, Tumor volumes from a A549 xenograft mouse model treated five times per week with 30 mg/kg (*S*)-JQ1 and/or twice

weekly with 25 mg/kg MTX from day 19. Means and standard deviations from eight mice per group. Asterisks indicate significance of 1-way ANOVA adjusted by Tukey's multiple comparison test (* $P < 0.05$; ** $P < 0.005$; *** $P < 0.0001$) **d**, Weight and of tumors at the end of the experiment (day 43). Means and standard deviations from eight mice per group. Asterisks indicate significance of 1-way ANOVA adjusted by Tukey's multiple comparison test ($P = 0.00000050$). **e**, Images of tumors at the end of the experiment (day 43).

Europe PMC Funders Author Manuscripts